

Contents

Preface

A Basics - Scattering

- A01** 100 years of Scattering and Beyond
Th. Brückel
- A02** Scattering Theory: Born Series
S. Blügel
- A03** Scattering Theory: Dynamical Theory
Y. Mokrousov
- A04** Interaction of X-rays, Neutrons and Electrons with Matter
D. DiVincenzo
- A05** Correlation Functions Measured by Scattering Experiments
R. Zorn

B Basics - Materials

- B01** Crystal Structures and Symmetries
G. Roth
- B02** The Structure of Complex Fluids
G. Gompper
- B03** Diffusion
J. K. G. Dhont
- B04** Elementary Excitations in Crystalline Matter: Phonons and Magnons
K. Schmalzl
- B05** Crystal Field Effects and Excitations
M. Ležaić, M. Schlupf
- B06** Dynamics of Macromolecules
R. Winkler

C Sources and Instrumentation

- C01** Neutron Sources
A. Ioffe
- C02** Synchrotron Radiation Sources
W. Eberhardt
- C03** Instruments for Neutron Scattering
M. Monkenbusch
- C04** Synchrotron X-ray Beamlines
U. Klemradt
- C05** X-Ray & Slow Neutron Detectors
G. Kemmerling
- C06** Polarized Neutron Scattering and Polarization Analysis
W. Schweika

- C07** Polarization Handling: Synchrotron
S. Nandi
- C08** The European X-ray Free-Electron Laser Project
M. Altarelli
- C09** The Road ahead for the European Spallation Source
C. Carlile

D Techniques

- D01** Small Angle Scattering and Large Scale Structures
H. Frielinghaus
- D02** Scattering under Grazing Incidence from Surfaces and Interfaces
U. Rücker
- D03** Powder and Single Crystal Diffractometry: Chemical and Magnetic Structures
M. Meven
- D04** Inelastic Scattering: Lattice, Magnetic and Electronic Excitations
J. Voigt
- D05** Atomic Pair Distribution Function: Local Structure Investigations
S. Disch
- D06** Critical Scattering at Phase Transitions
K. Nemkovski
- D07** Quasielastic Scattering
J. Wuttke
- D08** High Resolution Spectroscopy
G. Meier, M. Monkenbusch
- D09** Nuclear Resonance Scattering
R. Rüffer
- D10** Coherent Imaging with X-ray Free-Electron Lasers
H. N. Chapman
- D11** Anomalous and Resonant X-ray Scattering: Spin, Charge and Orbital Order
J. Stempfer

E Topical Applications

- E01** Superconductivity
Y. Xiao, Y. Su
- E02** Polymers: Structure
W. Pyckhout-Hintzen
- E03** Polymerdynamics
D. Richter
- E04** Material Systems for Information Technologies
M. Angst
- E05** Thin Film Heterostructures
E. Kentzinger, S. Pütter
- E06** Magnetic Nanoparticles
A. Feoktystov

E07 Energy Materials

R. Hermann

E08 Structure and Dynamics of Proteins

R. Biehl

E09 Glass Transition

U. Buchenau

E10 Protein Crystallography

T. Schrader

F Complementary Techniques

F01 Advanced Transmission Electron Microscopy Techniques and Applications

*R. Dunin-Borkowski, M. Feuerbacher, M. Heggen, L. Houben, A. Kovács,
M. Luysberg, A. Thus, K. Tillmann*

F02 Imaging with X-rays, Neutrons and Synchrotron Radiation

E. Lehmann

F03 Photoelectron Emission Spectroscopy

C. M. Schneider

F04 X-ray Absorption Spectroscopies

L. Baumgarten

Index

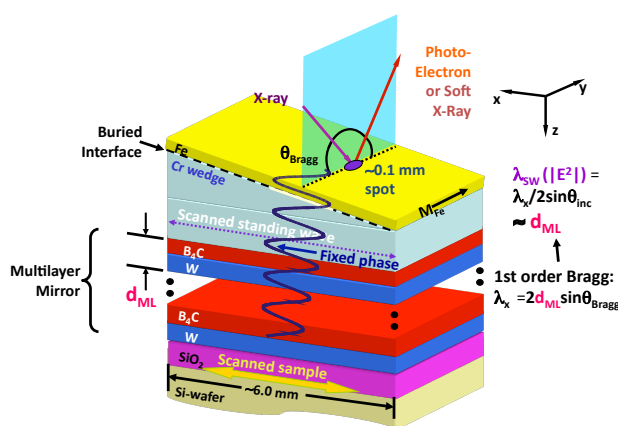


Figure 30: Schematic illustration of the simultaneous use of an x-ray standing wave plus a wedge-profile overlayer sample to selectively study buried interfaces and layers – the “swedge” method. In the example here, a strong standing wave (SW) is created by first-order Bragg reflection from a multilayer made of repeated B_4C/W bilayers, and a Cr wedge underneath an Fe overlayer permits scanning the SW through the Fe/Cr interface by scanning the sample along the x direction. From ref. [66].

wave is created by a typically well-focussed synchrotron radiation beam, then its dimensions will be much smaller than a typical sample, as indicated in the figure. Since the standing wave only exists in the region where the beam hits the sample surface, and its phase is locked tightly to the multilayer mirror, scanning the sample in the photon beam along the x direction effectively translates the standing wave through the sample. In the example shown, the standing wave would in particular scan through the Fe/Cr interface of interest, at some positions being more sensitive to the Fe side and at some more sensitive to the Cr side.

Some results obtained with this method for the Fe/Cr interface are summarized in Figs. 31 and 32. The analysis combined XPS intensity and MCDAD measurements (not shown here) from the 3p and 2p core levels of Fe and Cr, respectively. In Figure 31a is shown the variation of the Cr3p/Fe3p ratio as the sample is scanned in the way suggested above, for several angles of incidence near the Bragg angle. Oscillations in this ratio clearly reflect the passage of the standing wave node and belly through the interface. In Figure 31b we compile “rocking curves” in which the angle is varied around the Bragg angle for different positions x along the sample, or equivalently different Cr wedge thickness d_{Cr} . There are dramatic changes in the intensity ratio in this data also.

Self-consistently analyzing these data with x-ray optical calculations of standing-wave photoemission and only two variable parameters (the depth of onset of change in the Fe composition and the width of a linear gradient as the interface changes from pure Fe to pure Cr) yields the excellent fits shown to both types of data, and the parameters given at the left side of Figure 32a. The MCDAD data for both Fe 2p and Cr 2p core level photoemission have also been measured as the sample is scanned in the beam. The relative signs of the MCDAD signal for the Fe 2p and Cr 2p levels are found to be opposite [66]. This immediately implies that a small amount of Cr is oppositely magnetized compared to Fe, and this must be induced by the ferromagnetic Fe layer, since Cr is normally antiferromagnetic. Similar data have been obtained at the 3p levels of Cr and Fe. Further analyzing this data set with two parameters for Fe 2p and 3p MCD and two parameters for Cr 2p and 3p MCD yields the atom-specific magnetization profiles shown at right hand side of Figure 32a.

Thus, in the above described experiment the swedge method has permitted non-destructively determining the concentration profile through an interface, as well as the atom-specific magnetization contributions through it. The swedge approach has also been used successfully to determine layer-specific densities of states that can be linked changes in magnetoresistance as a function of nanolayer thicknesses [68]. Several other possible applications of it have also been